RESEARCH ARTICLE

Clinically Meaningful Magnetic Resonance Endpoints Sensitive to Preataxic Spinocerebellar Ataxia Types 1 and 3

Jayashree Chandrasekaran, MS,[1] Emilien Petit, MSc,[2] Young Woo Park, PhD,[1] Sophie Tezenas du Montcel, MD, PhD,[2] James M. Joers, PhD,[1] Dinesh K. Deelchand, PhD,[1] Michal Považan, PhD,[3] Guita Banan, PhD,[4] Romain Valabregue, PhD,[2] Philipp Ehses, PhD,[5] Jennifer Faber, MD,[5,6] Pierrick Coupé, PhD,[7] Chiadi U. Onyike, MBBS, MD,[3] Peter B. Barker, PhD,[3] Jeremy D. Schmahmann, MD,[8] Eva-Maria Ratai, PhD,[9] S. H. Subramony, MD,[4] Thomas H. Mareci, PhD,[4] Khalaf O. Bushara, MD,[10] Henry Paulson, MD, PhD,[11] Alexandra Durr, MD, PhD,[2] Thomas Klockgether, MD,[5,6] Tetsuo Ashizawa, MD,[12] Christophe Lenglet, PhD,[1] and Gülin Öz, PhD,[1] for the READISCA Consortium

Objective: This study was undertaken to identify magnetic resonance (MR) metrics that are most sensitive to early changes in the brain in spinocerebellar ataxia type 1 (SCA1) and type 3 (SCA3) using an advanced multimodal MR imaging (MRI) protocol in the multisite trial setting.

Methods: SCA1 or SCA3 mutation carriers and controls (n = 107) underwent MR scanning in the US-European READISCA study to obtain structural, diffusion MRI, and MR spectroscopy data using an advanced protocol at 3T. Morphometric, microstructural, and neurochemical metrics were analyzed blinded to diagnosis and compared between preataxic SCA (n = 11 SCA1, n = 28 SCA3), ataxic SCA (n = 14 SCA1, n = 37 SCA3), and control (n = 17) groups using nonparametric testing accounting for multiple comparisons. MR metrics that were most sensitive to preataxic abnormalities were identified using receiver operating characteristic (ROC) analyses.

View this article online at wileyonlinelibrary.com. DOI: 10.1002/ana.26573

Received Aug 3, 2022, and in revised form Nov 18, 2022. Accepted for publication Dec 6, 2022.

Address correspondence to Dr Öz, Center for Magnetic Resonance Research, University of Minnesota, 2021 Sixth Street Southeast, Minneapolis, MN 55455. E-mail: gulin@cmrr.umn.edu

Emilien Petit and Young-Woo Park contributed equally to this work.

From the [1]Center for Magnetic Resonance Research, Department of Radiology, University of Minnesota, Minneapolis, MN, USA; [2]Paris Brain Institute, Sorbonne University, National Institute of Health and Medical Research (Inserm), National Institute for Research in Digital Science and Technology (INRIA), National Center for Scientific Research (CNRS), Assistance Publique - Hôpitaux de Paris (APHP), Paris, France; [3]Department of Radiology and Radiological Science, Johns Hopkins University School of Medicine, Baltimore, MD, USA; [4]Norman Fixel Center for Neurological Disorders, College of Medicine, University of Florida, Gainesville, FL, USA; [5]German Center for Neurodegenerative Diseases, Bonn, Germany; [6]Department of Neurology, University Hospital Bonn, Bonn, Germany; [7]Laboratoire Bordelais de Recherche en Informatique (LaBRI), Bordeaux University, Bordeaux, France; [8]Ataxia Center, Laboratory for Neuroanatomy and Cerebellar Neurobiology, Department of Neurology, Massachusetts General Hospital and Harvard Medical School, Boston, MA, USA; [9]Athinoula A. Martinos Center for Biomedical Imaging, Massachusetts General Hospital, Charlestown, MA, USA; [10]Department of Neurology, University of Minnesota, Minneapolis, MN, USA; [11]Department of Neurology, University of Michigan, Ann Arbor, MI, USA; and [12]Stanley H. Appel Department of Neurology, Houston Methodist Research Institute, Houston, TX, USA

Additional supporting information can be found in the online version of this article.

Results: Atrophy and microstructural damage in the brainstem and cerebellar peduncles and neurochemical abnormalities in the pons were prominent in both preataxic groups, when patients did not differ from controls clinically. MR metrics were strongly associated with ataxia symptoms, activities of daily living, and estimated ataxia duration. A neurochemical measure was the most sensitive metric to preataxic changes in SCA1 (ROC area under the curve [AUC] = 0.95), and a microstructural metric was the most sensitive metric to preataxic changes in SCA3 (AUC = 0.92).
Interpretation: Changes in cerebellar afferent and efferent pathways underlie the earliest symptoms of both SCAs. MR metrics collected with a harmonized advanced protocol in the multisite trial setting allow detection of disease effects in individuals before ataxia onset with potential clinical trial utility for subject stratification.

ANN NEUROL 2022;00:1–16

Spinocerebellar ataxias (SCAs) are rare autosomal dominant neurodegenerative disorders, the clinical hallmark of which is progressive loss of balance and coordination. SCA1 is the fastest progressing,[1,2] and SCA3 the most common SCA worldwide.[3] Both are polyglutamine diseases caused by translated dynamic CAG repeat expansion mutations and present with degeneration in the cerebellum and brainstem. Disease-modifying therapies including gene silencing strategies are in the SCA therapeutic pipeline.[4] Effectiveness of such therapies is most likely when they are administered at early disease stages.[5] However, clinical outcome measures have low sensitivity in early disease, necessitating alternative measures to identify trial participants with cerebral and cerebellar changes before onset of ataxia. Noninvasive imaging may allow detection of such early degenerative changes in SCAs, and thereby facilitate trials at early disease stages.

Atrophy of the cerebellum, brainstem, and forebrain regions are reliably detected with structural MRI in SCAs,[6] including at an early stage at the group level.[7–9] In addition, microstructural damage to the white matter (WM) and neurochemical abnormalities that likely precede tissue loss were detectable at subject level in single site studies with few preataxic subjects using diffusion magnetic resonance imaging (MRI)[10,11] and magnetic resonance spectroscopy (MRS),[12,13] respectively. Hence, studies of larger trial-ready cohorts at the earliest disease stages with a multimodal imaging protocol are warranted.

READISCA[14] is a multinational longitudinal clinical trial readiness study that enrolls preataxic and early ataxic SCA1 and SCA3 mutation carriers[15] and matched healthy controls. READISCA enrolled the largest preataxic SCA cohorts for multimodal imaging thus far. Here we report the baseline structural, diffusion MRI, and MRS findings. Our goals were (1) to evaluate the feasibility of collecting multimodal magnetic resonance (MR) data using a harmonized advanced protocol in the multisite academic trial setting; (2) to identify the structural, microstructural, and neurochemical MR metrics that are most sensitive to early abnormalities in SCA1 and SCA3 mutation carriers; and (3) to investigate the associations of these MR metrics with early clinical presentation in SCA1 and SCA3 as assessed by a comprehensive battery of outcome measures covering motor, nonmotor, and cognitive function and activities of daily living.

Subjects and Methods

Study Participants and Design

The imaging cohort of READISCA included 107 participants who were willing to undergo MRI and clear of MR contraindications (Table). They were enrolled at 16 sites[14] in the United States and Europe from 2018 to 2021. The sample size was guided by feasibility to enroll preataxic and very early stage participants. Participants with a Scale for the Assessment and Rating of Ataxia (SARA)[16] score < 10 (range = 0–40; 0 indicates no ataxia and 40 most severe ataxia) were targeted for enrollment. SCA mutation carriers with SARA < 3 were classified as preataxic and those with SARA ≥ 3 as ataxic.[15,17] Control subjects consisted of at-risk individuals (first-degree relatives of patients) who tested negative for SCA1 or SCA3 and healthy volunteers who were unrelated to the patients. Individuals who were diagnosed with a hereditary ataxia other than SCA1 or SCA3, had a concomitant disorder that affected assessment of ataxia, had taken investigational drugs, or had changes in coordinative physical and occupational therapy 2 months prior to participation were excluded.

Participants underwent clinical evaluation at the enrolling sites and were scanned within 9 weeks (87 subjects within 4 weeks) at one of the 6 imaging sites in the United States (University of Minnesota, University of Florida, Johns Hopkins University, Massachusetts General Hospital) and Europe (German Center for Neurodegenerative Diseases, ICM Paris Brain Institute). Site selection was based on MR expertise, prior collaborations that enabled timely initiation of scans in parallel with clinical assessments, and availability of 3T Siemens scanners. All procedures were approved by the institutional review board at each site. Informed consent was obtained from all participants.

Clinical Assessments

All subjects underwent the SARA[16] assessment, which is a composite cerebellar ataxia scale, and was used to define the preataxic and ataxic groups as described above. Ataxic participants reported age at ataxia onset (see Table). In addition, time from ataxia onset was estimated using CAG repeat length for both preataxic and ataxic participants (using long alleles for SCA1[17] and both alleles with a newer improved statistical model for SCA3,[18] which does not display a systematic bias in patients with late onset ataxia observed with the original Tezenas formula, Tezenas

TABLE. Cohort Characteristics

Variable	Control (C)	SCA1 Preataxic (P)	SCA1 Ataxic (A)	SCA3 Preataxic (P)	SCA3 Ataxic (A)
n	17	11	14	28	37
Sex, female[a]	7 (41%)	8 (69%)	9 (67%)	19 (68%)	18 (49%)
Age, yr[a]	43 [34;51]	38 [34.5;45.5]	46.5 [36.5;54]	36 [31.75;41.25][b]	50 [42;57][b]
SARA	0 [0;1]	1 [0;1.9] (n = 10)	8.3 [7;9]	1.3 [0;2]	7 [5.5;8.5]
CAG repeat length, long allele		42 [41.5;43.5][c]	45 [43;46] (n = 13)[c]	70 [69;72.25]	71.5 [67;73] (n = 36)
CAG repeat length, short allele		29 [29;30]	29 [29;30] (n = 13)	23 [21;27]	23 [20;24] (n = 33)
Reported age at onset, yr			40 [35;47.5] (n = 11)		45 [37;48] (n = 33)
Reported time from ataxia onset, yr			6 [4;12] (n = 11)		3 [2;10] (n = 33)
Estimated time from ataxia onset, yr[d]		−7.01 [−9.18; −2.19][b]	5.38 [−0.56;12.29] (n = 13)[b]	−2.21 [−6.78;2.36][b]	9.36 [5.04;13.19] (n = 36)[b]
CCAS	108 [102;112]	101 [99;104] (n = 10)	95 [90;106] (n = 13)	101 [94;111] (n = 25)	96 [91;102] (n = 34)[e]
CCFS	0.878 [0.838;0.930] (n = 15)	0.872 [0.845;0.894] (n = 8)[b]	0.976 [0.930;1.030] (n = 12)[b,e]	0.851 [0.835;0.886] (n = 25)[b]	0.922 [0.864;0.982] (n = 35)[b]
PHQ-9	2.0 [0;3.0]	0.5 [0;3.5] (n = 10)	5.5 [1.5;8.8]	2.0 [0;4.0]	3.5 [1.0;6.3] (n = 36)
FARS-ADL	0 [0;1.0]	0 [0;1.0] (n = 10)[b]	4.0 [3.5;8.0] (n = 13)[b,e]	0.5 [0;1.8] (n = 27)[b]	4.0 [2.4;6.3] (n = 36)[b,e]
FARS-FS	0 [0;0] (n = 15)	0 [0;0] (n = 9)[b]	2 [1.5;2][b,e]	0 [0;1][b]	2 [1;2][b,e]
EQ-5D	90 [80;90]	90 [81;96] (n = 10)	80 [71;89]	90 [80;98][b]	80 [70;85] (n = 36)[b]
INAS	0 [0;1]	1 [0;2] (n = 10)	2 [1;2][e]	1 [0;2][b]	3 [2;4][b,e]

For qualitative variables frequencies are provided using percentages, and for quantitative variables median and interquartile range [Q1;Q3] are provided; n is provided when values are missing.

CCAS = Cerebellar Cognitive Affective Syndrome Scale; CCFS = Composite Cerebellar Functional Severity Score; EQ-5D = European Quality of Life–5 Dimensions; FARS-ADL = Friedreich's Ataxia Rating Scale Activities of Daily Living; FARS-FS = Friedreich's Ataxia Rating Scale Functional Staging; INAS = Inventory of Non-Ataxia Signs; PHQ-9 = Patient Health Questionnaire 9; SARA = Scale for the Assessment and Rating of Ataxia; SCA = spinocerebellar ataxia.

[a]No significant differences were observed in age and sex between the SCA groups and healthy controls.

[b]$p < 0.01$ for pairwise comparison between P and A within a SCA group.

[c]$p < 0.05$ for pairwise comparison between P and A within an SCA group.

[d]Estimated time from onset (ataxia duration) was calculated for both preataxic and ataxic SCA groups using CAG repeat length.

[e]$p < 0.01$ for pairwise comparison between C and A.

du Montcel et al, Neurology, in press). All participants underwent the clinical outcome assessments (COAs) of READISCA, including the Composite Cerebellar Functional Severity Score (CCFS),[19] Inventory of Non-Ataxia Signs (INAS),[20] Cerebellar Cognitive Affective Syndrome Scale (CCAS),[21] Friedreich's Ataxia Rating Scale Activities of Daily Living (FARS-ADL) and Functional Staging (FARS-FS) subscales,[22] Patient Health Questionnaire 9 (PHQ-9),[23] and the European Quality of Life–5 Dimensions (EQ-5D) visual analogue scale.[24] The COAs that showed significant group differences in the entire READISCA cohort (n = 200; Tezenas du Montcel et al, Neurology, in press) are summarized for the MR cohort in the Table .

MRI Data Acquisition

MR data were acquired on 3T Siemens (Erlangen, Germany) scanners (5 Prisma, 1 Skyra) operating under Syngo MR E11 software and using body coil transmission and a 32-channel receive array. Structural and diffusion MRIs were acquired with the Human Connectome Project (HCP) Lifespan protocol: (1) 3-dimensional (3D) T_1-weighted magnetization-prepared rapid acquisition gradient echo ($0.8mm^3$ isotropic resolution, repetition time [TR] = 2,400 milliseconds, echo time [TE] = 2.22 milliseconds, inversion time = 1,000 milliseconds, flip angle = 8°, generalized autocalibrating partially parallel acquisition [GRAPPA] factor = 2); (2) 3D T_2-weighted SPACE (sampling perfection with application-optimized contrasts using different flip angle evolution; $0.8mm^3$ isotropic resolution, TR/TE = 3200/563 milliseconds, GRAPPA factor = 2); (3) multiband diffusion MRI acquired with opposing phase encoding in the anterior–posterior direction and *q* space sampling split into 2 sets of 98 and 2 sets of 99 volumes, resulting in 2 sets of 197 volumes including 13 b = 0 per phase encode (184 unique diffusion images). On Prisma scanners, $1.5mm^3$ isotropic resolution, TR/TE = 3,230/89.2 milliseconds, multiband acceleration = 4, and b values = 1,500, 3,000 s/mm^2 were used. On the Skyra scanner, $1.7mm^3$ isotropic resolution, TR/TE = 3,390/103.2-milliseconds, multiband acceleration = 4, and b values = 1,000, 2,000 s/mm^2 were used. Except b values, *q* space sampling was the same on Prisma and Skyra.

Volumes-of-interest (VOIs) for MRS were pons ($16 \times 16 \times 16mm^3$) and cerebellar WM (CBWM; $17 \times 17 \times 17mm^3$). VOIs were automatically prescribed with AutoVOI, using predefined voxels on the MNI152 atlas.[25] MRS data were collected using semilocalization by adiabatic selective refocusing (sLASER; TR/TE = 3,000/30 milliseconds, 80 transients),[26] which was recommended by expert consensus for high fields.[27] Unsuppressed water spectra were obtained as an internal quantification reference and for residual eddy current correction.[28] An automated sLASER protocol[29] with integrated B_0 and B_1 calibration minimized operator intervention.

MR Quality Control and Preprocessing

Digital Imaging and Communications in Medicine (DICOM) data were deidentified using DicomBrowser,[30] and T_1 and T_2 datasets were defaced using Face Masking[31] on site prior to uploading to a Flywheel (https://flywheel.io/) instance running on a dedicated server at the University of Minnesota for centralized analysis. To ensure uniform data handling across sites, the data handling pipeline was created within a Docker container at the University of Minnesota and shared with other imaging sites.

All MR data were analyzed blinded to diagnosis. Image sharpness, ringing, and contrast-to-noise ratio of T_1 and T_2 data were scored 0–2 in subcortical, gray matter (GM), and WM regions, as described previously.[32] Scores for all image features were averaged. T_1 and T_2 images that passed quality control (QC) thresholds (pass = 0–0.25, check = 0.5–1, fail = 1.25–2) were preprocessed using the HCP minimal preprocessing pipelines[33] and corrected for gradient nonlinearity distortion, bias field, and readout distortions.[33]

Diffusion data were missing for 2 participants, and another was excluded due to motion artifacts. Diffusion images were corrected for motion artifacts, and susceptibility-induced and eddy current distortions[34] using the HCP pipelines.[33] Three datasets did not include reversed phase-encoding direction due to operator error, and thus were corrected for susceptibility-induced distortions using Synb0-DISCO[35] and for eddy current and motion artifacts using EDDY from FSL.[34]

MRS data were missing for 2 participants. In addition, MRS data were excluded if the VOIs were misplaced when overwriting AutoVOI placement (1 pons spectrum, 3 CBWM spectra) or the linewidth (full width at half maximum) of the associated water reference was broader than 13Hz (11 pons spectra and 3 CBWM spectra). MRS DICOM files containing channel-combined single-shot sLASER spectra were corrected for frequency, phase, and eddy current errors in an automated pipeline[36] using MRspa (https://www.cmrr.umn.edu/downloads/mrspa/) before averaging. Single shots with poor water suppression or phase fluctuation indicating subject movement were excluded from averaging.

Volumetry

Cortical, subcortical, and brainstem volumes were estimated using FreeSurfer (v6.0).[37,38] Because FreeSurfer only provides white and GM segmentations of the cerebellum, CERES (CEREbellum Segmentation, v1.0), a patch-based multi-atlas segmentation tool,[39] was used to estimate cerebellar lobule volumes. CERES was chosen for cerebellar segmentation because it outperformed other tools with respect to repeatability and reproducibility[40] and cerebellar fissure segmentation in images with cerebellar atrophy.[41] All volumes were normalized by each participant's total intracranial volume.

Region of Interest-Based Diffusion Analysis

To minimize bias from differences in *b* values and voxel sizes[42] between Prisma and Skyra platforms, diffusion volumes with b = 1500 s/mm^2 for Prisma and b = 1000 s/mm^2 for Skyra were extracted for diffusion tensor calculation. Fractional anisotropy (FA), mean diffusivity (MD), axial diffusivity (AD), and radial diffusivity (RD) were subsequently calculated using FSL DTIFIT (FSL v6.0) in 25 WM regions of interest (ROIs) for each subject in their native space as previously described.[11] For the list and visualization of the 25 ROIs, see the first figure in our prior publication.[11]

A bias was noted in the diffusivity values in the Skyra (up to 20% higher) compared to Prisma data. To address this,

diffusion data were acquired with the Prisma and Skyra protocols in the same session on a Prisma scanner from 3 healthy volunteers. AD, MD, and RD were computed from the same 25 WM ROIs. ROI-specific diffusivity scaling factors (diffusivity obtained with Prisma parameters divided by diffusivity obtained with Skyra parameters) were computed using average data from the 3 volunteers and ranged from 0.82 to 0.95. Skyra diffusivity values were then multiplied by the corresponding scaling factor. Statistical analysis was completed with both corrected and uncorrected Skyra diffusivities and with and without the Skyra data.

MRS Quantification

Preprocessed, averaged spectra were quantified using a simulated basis set[28] in LCModel (6.3.0G).[43] Metabolite concentrations were corrected for water T_2 relaxation time, tissue water content, and cerebrospinal fluid contribution in each VOI.[13] For each VOI, metabolites with mean Cramér–Rao lower bounds (CRLBs) ≤ 20% (estimated error of metabolite quantification) for the entire cohort were included in the statistical analyses. All concentrations except those for which the fitting failed (CRLB = 999%) were used when calculating mean CRLBs. For metabolites with strong correlations ($r < -0.7$), only the sum was reported, for example, total *N*-acetylaspartate (tNAA) = *N*-acetylaspartate + *N*-acetylaspartylglutamate, total creatine (tCr) = creatine + phosphocreatine, total choline = phosphocholine + glycerophosphocholine. Finally, glucose (Glc) + taurine (Tau) was reported if Glc or Tau had mean CRLB > 20%.[12]

Statistical Analysis

MR and clinical data from control, preataxic, and ataxic groups were compared using nonparametric Kruskal–Wallis test. SARA scores were only compared between control and preataxic groups, because SARA was used to classify preataxic and ataxic groups. Probability values were Holm adjusted for multiple comparisons within each MR analysis (for 55 volumes in FreeSurfer volumetry, 26 volumes in CERES volumetry, 25 regions in each diffusion metric, 19 metabolites in MRS across both VOIs). The metrics that showed statistical significance ($p < 0.05$) in the group comparisons underwent pairwise comparisons between the 3 groups in the SCA1 and SCA3 cohorts separately using 2-tailed *t* tests with Dunn adjustment for multiple pairwise comparisons. Cohen d was computed for each group comparison as the difference in means divided by the pooled standard deviation, which was calculated as the square root of the mean of each group's variance.

The MR metrics that best distinguished preataxic and control groups were identified using receiver operating characteristic (ROC) analyses. Optimal cutoff for the variables was determined using the Youden statistic that optimized specificity and sensitivity. The area under the curve (AUC) was calculated for each metric in both SCA1 and SCA3 groups. To assess the potential of multimodal MR metrics in identifying abnormalities at the preataxic stage, bivariate ROC analysis was done for SCA3 only (and not for SCA1 due to small sample size in the preataxic group, n < 15).

Pearson correlations between clinical and MR measures that showed significant group differences were computed for SCA1 and SCA3 using all participants' data, as well as without the control group. There were no group effects or nonlinearity that could be visually identified. For diffusivity metrics (AD, RD, MD), we only computed correlations of MD with COAs, because it is representative of both AD and RD and showed the largest number of group differences.

The clinical and imaging data from READISCA are available from the National Institute of Mental Health Data Archive (https://nda.nih.gov/, Collection C3155).

Results

Cohort Characteristics and Matching

Consistent with the reported[3] prevalence of SCA3, ~70% of SCA mutation carriers had SCA3 (n = 65) and ~ 30% had SCA1 (n = 25), with 43 to 44% at the preataxic stage (see Table). The control group was age- and sex-matched to mutation carriers. As expected, ataxic patients were older than preataxic participants, which was statistically significant for SCA3. Ataxic participants had mild symptoms and minimal disability (median SARA = 7–8; functional stage = 2). They had ataxia symptoms for 3 to 6 years. Ataxic groups scored worse than controls on FARS-FS, INAS count, and FARS-ADL subscale. CCFS was significantly different from controls only in the SCA1 ataxic group, and CCAS only in the SCA3 ataxic group. None of the COAs differed significantly between preataxic and control groups.

Early Atrophy in SCA1 and SCA3

All structural images passed the QC threshold (score ≤ 1). The regions that showed significant pairwise differences between ataxic groups and controls on structural MRI were identical to the regions with significant differences in the 3-group comparisons (shown in the top 2 rows of each panel in Fig 1), with lower *p* values (Supplementary Tables S1 and S4). Cerebellar WM, medulla, pons, and superior cerebellar peduncle (SCP) were atrophied in both ataxic groups. In addition, the SCA3 ataxic group had atrophy of the thalamus, nucleus accumbens, putamen, pallidum, and total and subcortical (striatum, thalamus, pallidum) GM. The medulla and SCP were already atrophied at the preataxic stage. In addition, the SCA1 preataxic group had atrophy of the pons and left cerebellar WM, and the SCA3 preataxic group displayed enlarged 4th ventricle.

Both ataxic groups had atrophy of cerebellar lobule IV. In addition, the SCA3 ataxic group showed atrophy of lobule X and left lobule I/II, with lobule X atrophied at the preataxic stage.

Early Microstructural Deficits in SCA1 and SCA3

Diffusivity findings were largely identical with and without the Skyra data and with the corrected and uncorrected

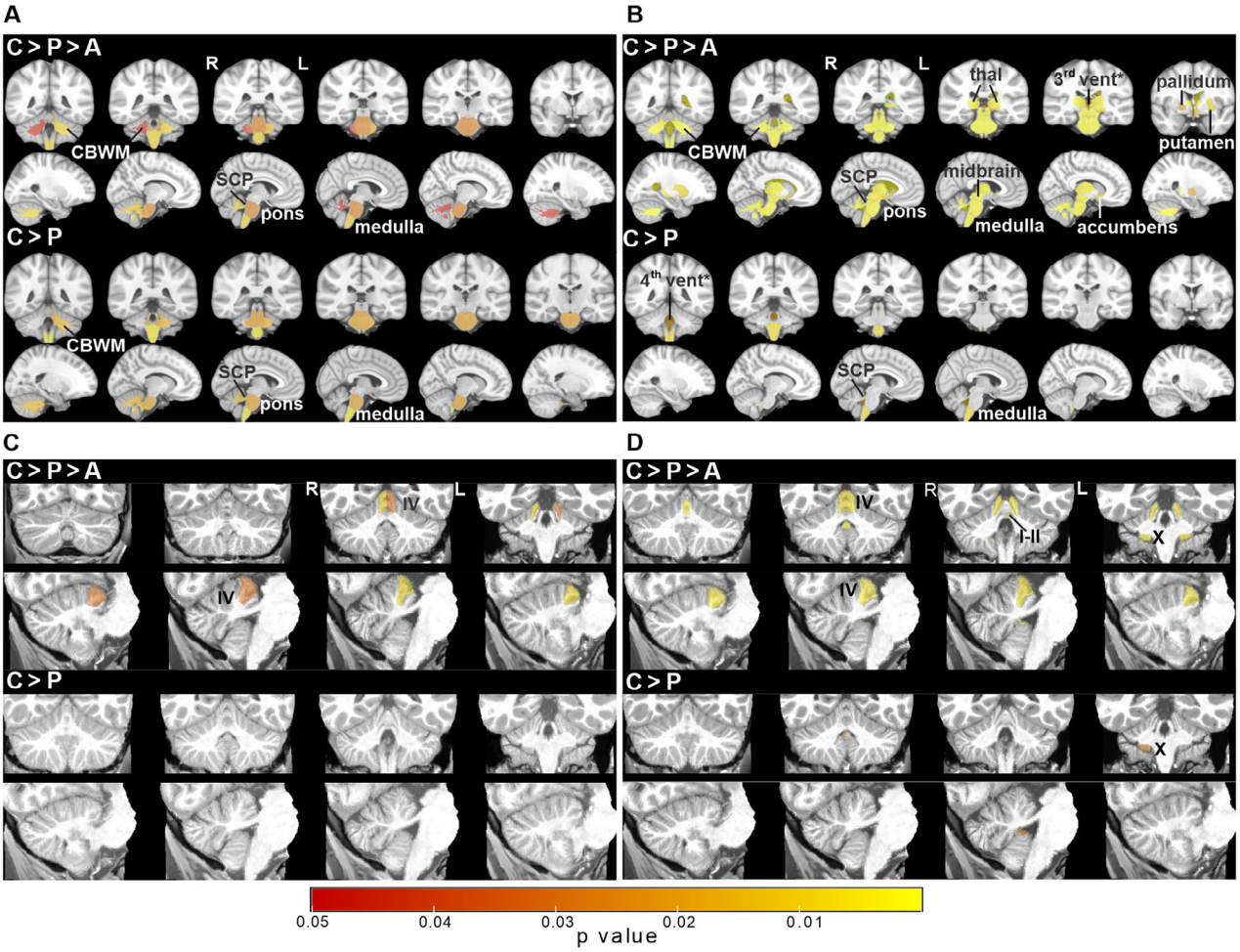

FIGURE 1: Whole brain and cerebellar volumetry. Statistical maps of whole brain volumetry using FreeSurfer (A, B) and cerebellum volumetry using CERES (C, D) for spinocerebellar ataxia type 1 (SCA1; A, C) and SCA3 (B, D) are shown. Group comparisons are shown in the top 2 rows and pairwise comparisons are shown in the bottom 2 rows in each panel. The *p* values (Kruskal–Wallis with Holm adjustment for C-P-A group comparisons, pairwise 2-tailed *t* tests for P vs C comparisons, $p < 0.05$) are mapped to each of the segmented volumes that are placed on a T1 atlas for whole brain volumetry. Similarly, *p* values from cerebellar volumetry are placed on a subject T1 image that was transformed to Montreal Neurological Institute space. Ventricles marked with an asterisk indicate reversed relationship between groups, that is, C < P < A. A = ataxic; C = control; CBWM = cerebellar white matter; L = left; P = preataxic; R = right; SCP = superior cerebellar peduncles; thal = thalamus; vent = ventricle.

Skyra values; therefore, we report the statistical findings with the corrected Skyra diffusivities. Similar to volumetric findings, the regions that showed significant pairwise differences between ataxic groups and controls in diffusion MRI were identical to the regions with significant differences in the 3-group comparisons (shown in the top 2 rows of each panel in Fig 2), with lower *p* values (Supplementary Tables S2 and S5).

Both ataxic groups displayed WM microstructural deficits in the pontine crossing tract (PCT) and cerebellar peduncles (inferior cerebellar peduncle [ICP], SCP, middle cerebellar peduncle) as measured by lower FA and higher diffusivities than controls (see Fig 2 and Supplementary Tables S2 and S5). In addition, corticospinal tract (CST), sagittal stratum (SS), and corona radiata (CR) were affected in both ataxic groups based on higher diffusivities. Corpus callosum (CC) was only affected in ataxic SCA1 (lower FA, higher MD and RD), whereas external capsule and internal capsule (IC) were only affected in ataxic SCA3 (higher RD/MD).

PCT and ICP were affected in both preataxic groups. In addition, the SCA3 preataxic group displayed widespread microstructural damage, including all cerebellar peduncles, CR, CST, IC, and SS (see Fig 2).

Early Neurochemical Abnormalities in SCA1 and SCA3

MRS data quality was high across groups, with comparable signal-to-noise ratio and linewidths between patients and controls (Tables S3 and S6).

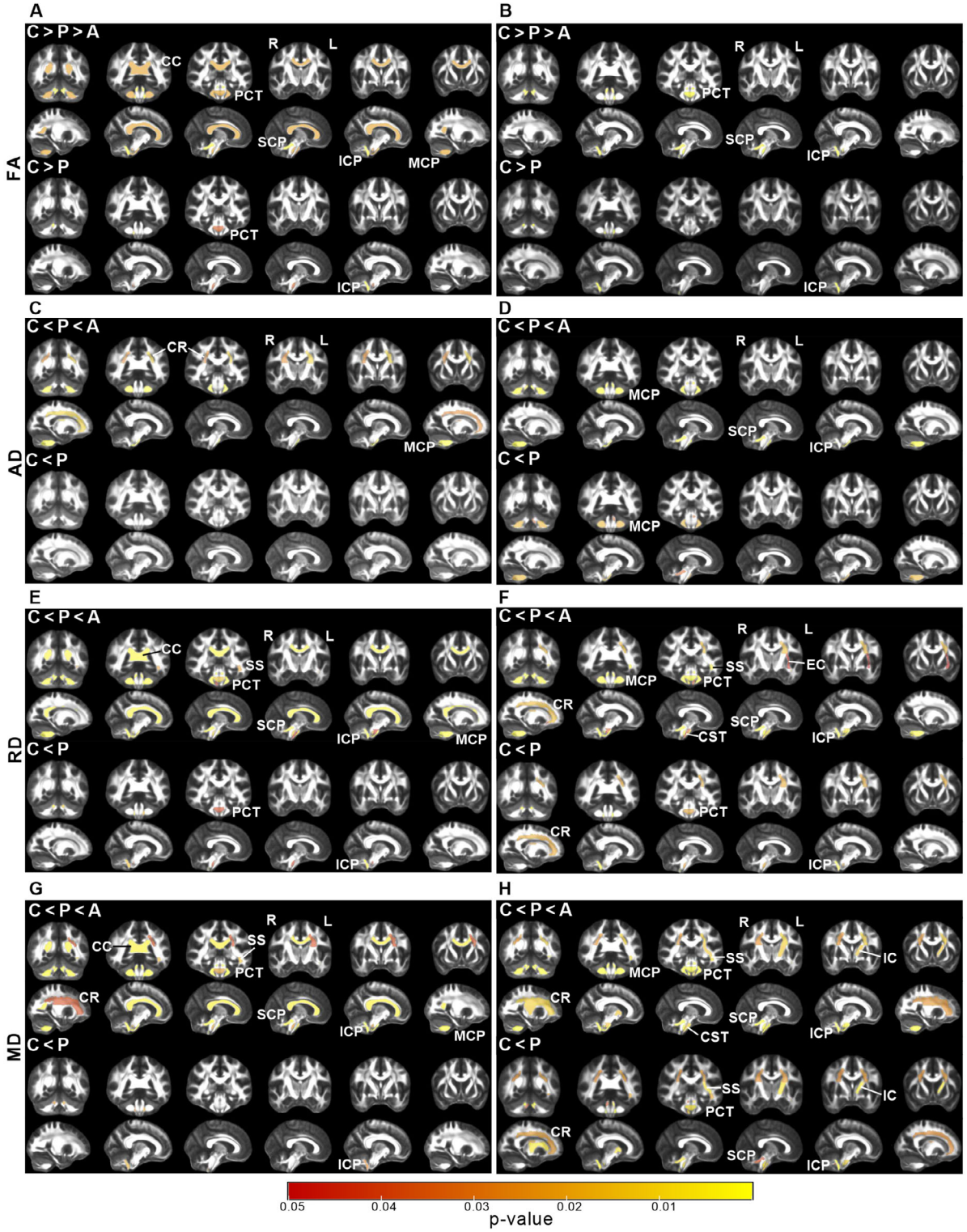

FIGURE 2: Microstructural magnetic resonance imaging (MRI) metrics from different regions of interest (ROIs). Statistical maps of ROI-based diffusion MRI analyses show significant differences in fractional anisotropy (FA; A, B), axial diffusivity (AD; C, D), radial diffusivity (RD; E, F), and mean diffusivity (MD; G, H) for spinocerebellar ataxia type 1 (SCA1; A, C, E, G) and SCA3 (B, D, F, H). Group comparisons are shown in the top 2 rows and pairwise comparisons are shown in the bottom 2 rows in each panel. The *p* value maps (Kruskal–Wallis with Holm adjustment for C-P-A group comparisons, pairwise 2-tailed *t* tests for P vs C comparisons, $p < 0.05$) are represented on white matter ROIs on the FMRIB58 atlas FA map. A = ataxic; C = control; CC = corpus callosum; CR = corona radiata; CST = corticospinal tract; EC = external capsule; IC = internal capsule; ICP = inferior cerebellar peduncle; MCP = middle cerebellar peduncle; P = preataxic; PCT = pontine crossing tract; SCP = superior cerebellar peduncle; SS = sagittal stratum.

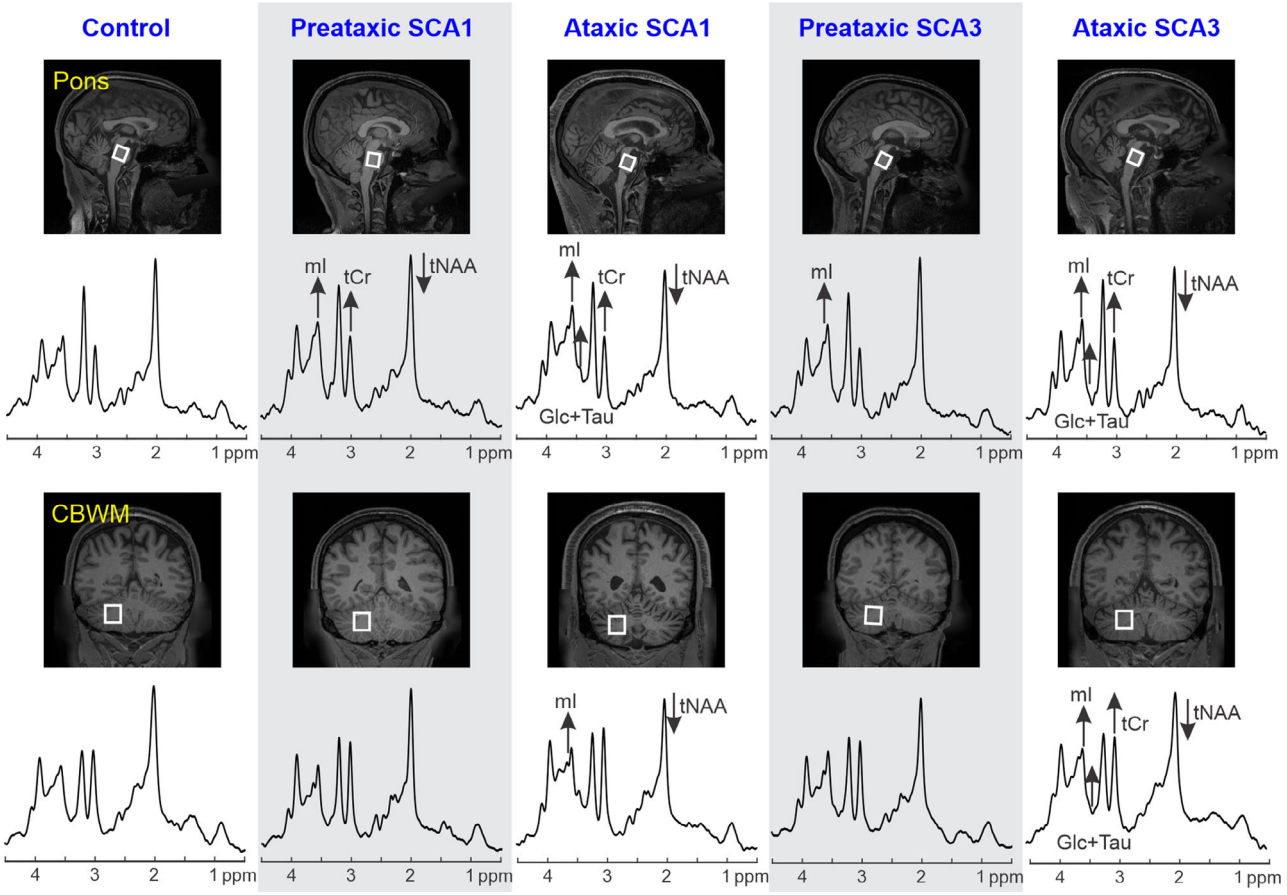

FIGURE 3: Neurochemical abnormalities from magnetic resonance (MR) spectra. MR spectra from 1 subject in each cohort are shown. Voxel positions are shown on magnetization-prepared rapid acquisition gradient echo images. Arrows indicate type I error corrected significant metabolite differences in each spinocerebellar ataxia (SCA) group compared to controls. CBWM = cerebellar white matter; Glc = glucose; mI = *myo*-inositol; Tau = taurine; tCr = total creatine; tNAA = total *N*-acetylaspartate.

Group differences for multiple neurochemicals were highly statistically significant for both SCAs, particularly for the pons. For both ataxic groups, levels of tNAA, a marker of neuronal viability, was lower and *myo*-inositol (mI), a putative glial marker, was higher than controls in both VOIs (Fig 3). In addition, tCr and Glc + Tau, which may indicate deficits in energy metabolism, were higher in both VOIs in ataxic SCA3 and in pons in ataxic SCA1 than controls.

Neurochemical differences reached statistical significance only in the pons at the preataxic stage. Namely, mI was higher in both preataxic groups than controls. Preataxic SCA1 participants further had lower tNAA and higher tCr than controls. In addition, tNAA/tCr and tNAA/mI ratios, which are widely used measures of neuroglial status, were lower in the pons in both preataxic groups.

MR Metrics Most Sensitive to Preataxic Disease

ROC analyses were used to identify the metrics most sensitive (highest AUC) to preataxic alterations within each modality (whole brain volumetry, cerebellar volumetry, diffusion MRI and MRS; Fig 4).

In SCA1, pontine tCr had the highest AUC (0.95) among the top metrics to distinguish preataxic participants from controls. Consistently, violin plots with individual subject data showed little overlap between the pontine tCr levels of the preataxic and control groups and largely equivalent tCr levels in the preataxic and ataxic groups.

In SCA3, RD of ICP had the highest AUC (0.92), and, similar to tCr in SCA1, the ICP RD values for the SCA3 preataxic and ataxic groups largely overlapped. Combinations of two MR metrics distinguished preataxic participants from controls with higher AUC than single metrics (Table S7). For example, the combination of ICP FA and cerebral peduncle AD resulted in almost perfect separation of preataxic participants from controls, with an AUC of 0.97.

Clinical Correlations

In SCA1, ataxia symptoms (SARA, FARS-FS) were significantly associated with volumes and microstructural

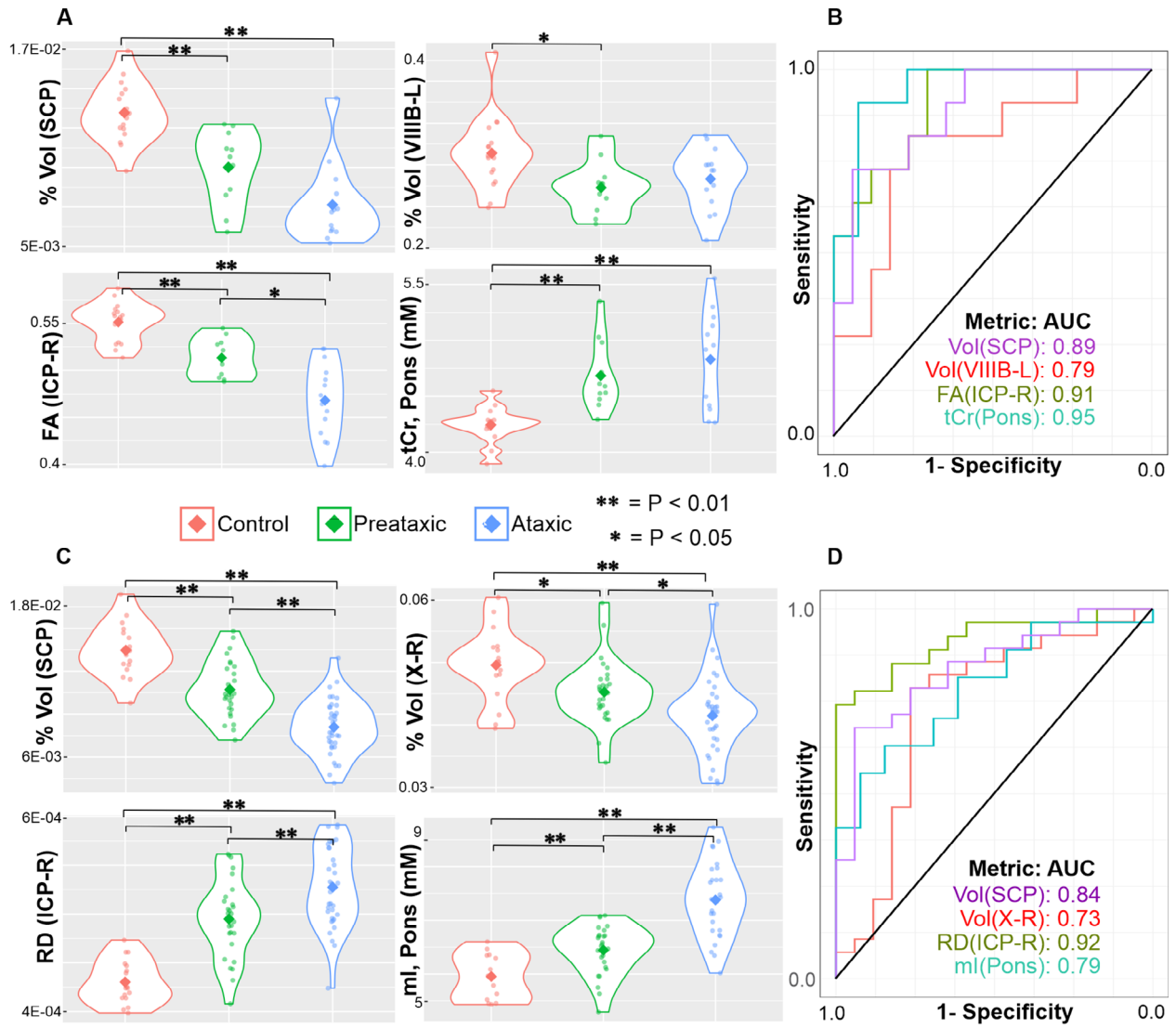

FIGURE 4: Magnetic resonance metrics most sensitive to preataxic alterations as identified from receiver operating characteristic (ROC) analyses. Violin plots (A, C) and ROC curves (B, D) are shown for the top volumetry (whole brain and cerebellar), diffusion, and magnetic resonance spectroscopy metrics that best distinguish preataxic spinocerebellar ataxia type 1 (SCA1; A, B) and SCA3 (C, D) groups from controls. Violin plots are shown for all groups (ataxic, preataxic SCA, and control) with 2-tailed *t* tests of pairwise comparison *p* values reported, whereas ROC analyses included control and preataxic groups only. Area under the curve (AUC) for each metric is indicated in the ROC plots. * = *p* <0.05; ** = *p* <0.01; FA = fractional anisotropy; ICP = inferior cerebellar peduncle; L = left; mI = *myo*-inositol; RD = radial diffusivity; SCP = superior cerebellar peduncle; tCr = total creatine; VIIIB = lobule VIIIB of cerebellum; Vol = volume; X = lobule X of cerebellum.

measures from brainstem (pons, medulla), cerebellum, and their connecting pathways, with the strongest associations detected for cerebellar peduncles ($|r|$ = 0.76–0.8; Fig 5). The strongest neurochemical correlates of ataxia were the neuronal marker tNAA ($|r| \sim 0.71$–0.79), followed by the glial marker mI ($r \sim 0.62$–0.76). MR metrics were also associated with fine motor function (CCFS), nonataxia signs (INAS), and estimated ataxia duration. Among patient-reported outcomes, the FARS-ADL scale showed the same pattern of associations with MR metrics as SARA and FARS-FS, whereas the EQ-5D and depression/anxiety (PHQ-9) scales lacked these associations. Finally, the cognitive and affective symptoms as measured by the CCAS showed moderate associations ($|r| \sim 0.3$–0.4) with CBWM volume, SCP and CC microstructure, and the glial marker mI.

Many clinical–MR associations were observed in the larger SCA3 sample (Fig 6). Similar to SCA1, macro- and microstructural metrics in the brainstem, particularly the pons, and cerebellar peduncles were the strongest correlates of ataxic symptoms (SARA, FARS-FS), fine motor skills (CCFS), nonataxia signs (INAS), FARS-ADL, and estimated ataxia duration. Importantly, volumes of several forebrain structures (thalamus, putamen, nucleus

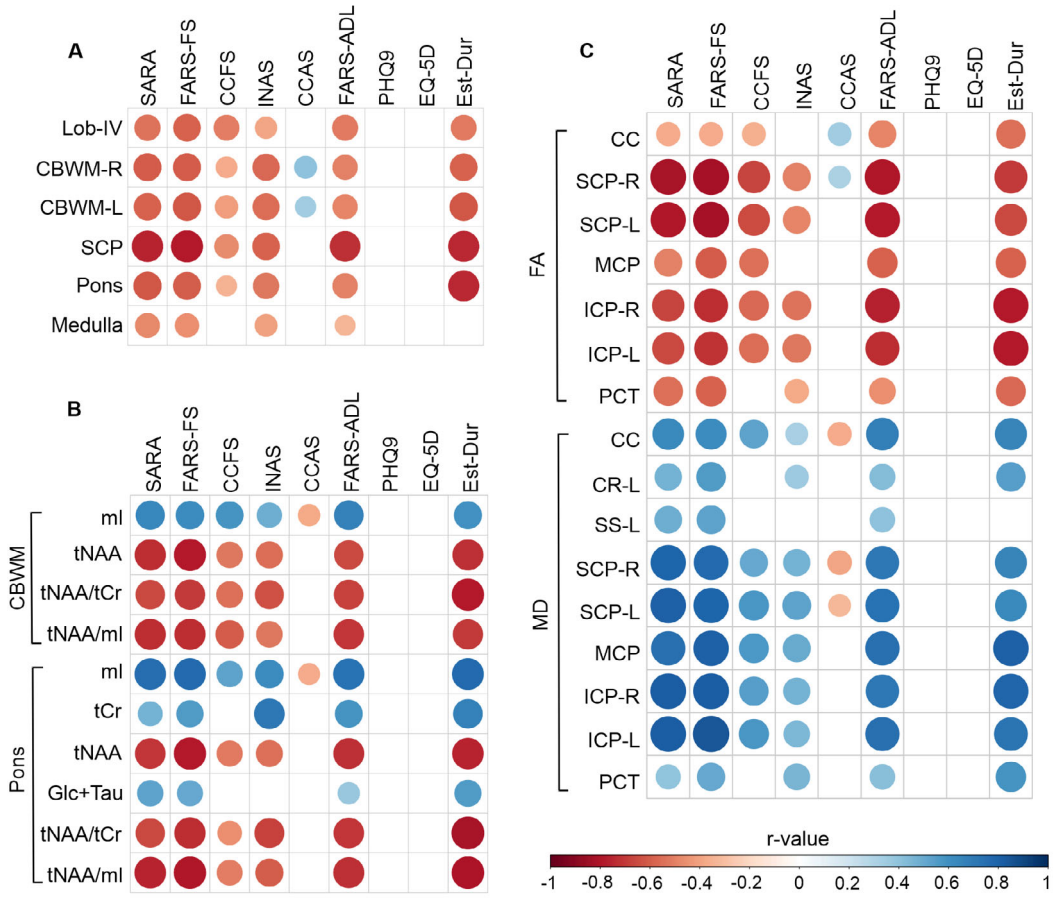

FIGURE 5: Associations of magnetic resonance and clinical metrics in spinocerebellar ataxia type 1 (SCA1). Statistically significant ($p < 0.05$) Pearson correlations between clinical outcome assessments and volumetric (A), neurochemical (B), and microstructural (C) metrics are shown. Correlation coefficients (r) were computed using all participants' data (ataxic SCA1, preataxic SCA1, controls) and are color coded as indicated by the legend bar. The size of the circles also indicates strength of the correlation. CBWM = cerebellar white matter; CC = corpus callosum; CCAS = Cerebellar Cognitive Affective Syndrome Scale; CCFS = Composite Cerebellar Functional Severity Score; CR = corona radiata; EQ-5D = European Quality of Life–5 Dimensions; Est-Dur = estimated ataxia duration; FA = fractional anisotropy; FARS-ADL = Friedreich's Ataxia Rating Scale Activities of Daily Living; FARS-FS = Friedreich's Ataxia Rating Scale Functional Staging; Glc = glucose; ICP = inferior cerebellar peduncle; INAS = Inventory of Non-Ataxia Signs; L = left; Lob-IV = lobule IV of cerebellum; MCP = middle cerebellar peduncle; MD = mean diffusivity; ml = *myo*-inositol; PCT = pontine crossing tract; PHQ9 = Patient Health Questionnaire 9; R = right; SARA = Scale for the Assessment and Rating of Ataxia; SCP = superior cerebellar peduncle; SS = sagittal stratum; Tau = taurine; tCr = total creatine; tNAA = total *N*-acetylaspartate.

accumbens) and diffusivity of major cerebral WM tracts (CR, CST) were associated with ataxia symptoms, nonataxia signs, and FARS-ADL. The larger sample also revealed associations of cerebellar and brainstem macro- and microstructure with cognitive and affective symptoms (CCAS), and of pons and cerebellar peduncle measures with quality of life (EQ-5D) and depression/anxiety (PHQ-9). Neurochemical associations with ataxia symptoms, nonataxia signs, patient-reported outcomes (FARS-ADL, EQ-5D, PHQ-9), and estimated ataxia duration were overall stronger than those of the structural and microstructural metrics.

The pattern of associations was similar without the control data, but associations were weaker. Correlations were not driven by cluster effects, as shown for SARA, FARS-FS, FARS-ADL, and estimated duration, the strongest clinical correlates of MR metrics overall (Fig 7). Diffusion tensor imaging (DTI) and MRS metrics had the strongest associations with these COAs.

Discussion

This study represents the first multisite clinical trial readiness effort in SCAs to validate morphometric, microstructural, and neurochemical outcome measures using an advanced MR protocol. The data expand our current knowledge on the earliest structural, microstructural, and neurochemical abnormalities that are present prior to

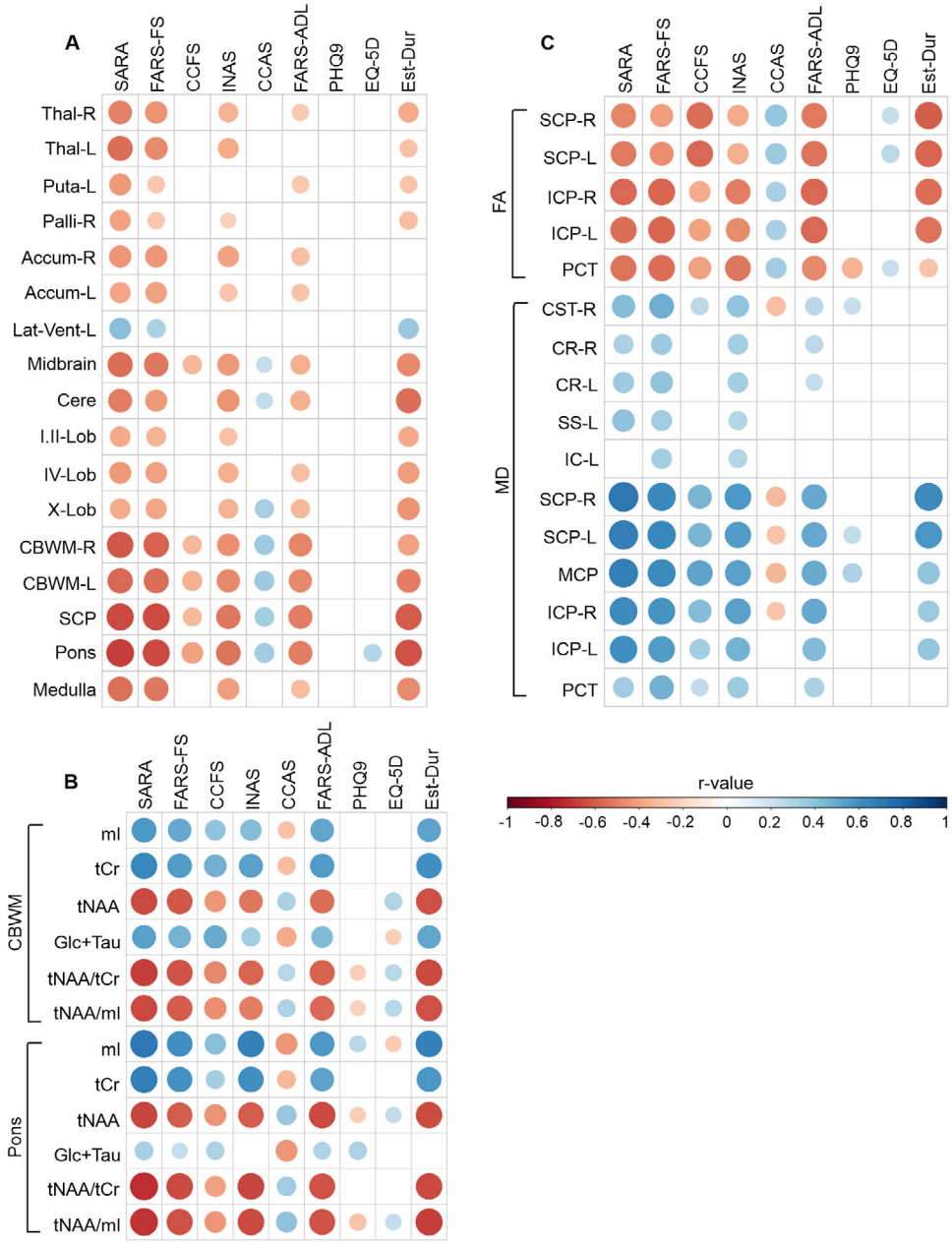

FIGURE 6: Associations of magnetic resonance and clinical metrics in spinocerebellar ataxia type 3 (SCA3). Statistically significant ($p < 0.05$) Pearson correlations between clinical outcome assessments and volumetric (A), neurochemical (B), and microstructural (C) metrics are shown. Correlation coefficients (r) were computed using all participants' data (ataxic SCA3, preataxic SCA3, controls) and are color coded as indicated by the legend bar. The size of the circles also indicates strength of the correlation. Accum = nucleus accumbens; CBWM = cerebellar white matter; CCAS = cerebellar cognitive-affective syndrome; CCFS = composite cerebellar functional severity score; Cere = cerebellum; CR = corona radiata; CST = corticospinal tract; EQ-5D = European Quality of Life–5 Dimensions; Est-Dur = estimated ataxia duration; FA = fractional anisotropy; FARS-ADL = Friedreich's Ataxia Rating Scale Activities of Daily Living; FARS-FS = Friedreich's Ataxia Rating Scale Functional Staging; Glc = glucose; I.II-Lob = lobule I & II of cerebellum; IC = internal capsule; ICP = inferior cerebellar peduncle; INAS = Inventory of Non-Ataxia Signs; IV-Lob = lobule IV of cerebellum; L = left; Lat-Vent = lateral ventricle; MCP = middle cerebellar peduncle; MD = mean diffusivity; ml = *myo*-inositol; Palli = pallidum; PCT = pontine crossing tract; PHQ9 = Patient Health Questionnaire 9; Puta = putamen; R = right; SARA = Scale for the Assessment and Rating of Ataxia; SCP = superior cerebellar peduncle; SS = sagittal stratum; Tau = taurine; tCr = total creatine; Thal = thalamus; tNAA = total *N*-acetylaspartate; X-Lob = lobule X of cerebellum.

ataxia onset and demonstrate WM damage that precedes GM damage in both SCAs. Thus, this is the first report of microstructural abnormalities in major WM tracts beyond the cerebellum and brainstem before ataxia onset in SCA3. From the trial readiness perspective, this is the first demonstration that neurochemical (for SCA1) and

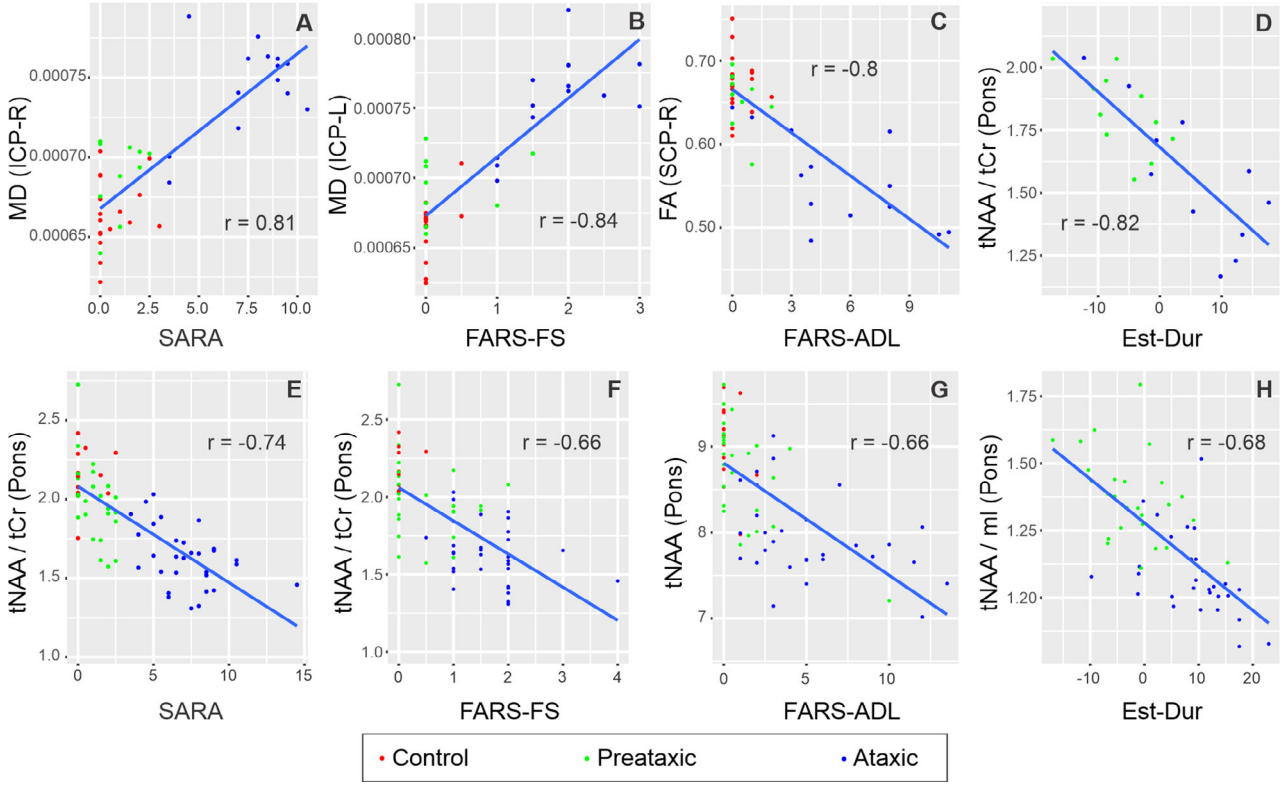

FIGURE 7: The strongest magnetic resonance (MR) correlates of Scale for the Assessment and Rating of Ataxia (SARA), functional stage, activities of daily living, and estimated disease duration in spinocerebellar ataxia type 1 (SCA1) and SCA3. Pearson correlations of MR metrics with the highest correlation coefficient with each of SARA, Friedreich's Ataxia Rating Scale Functional Staging (FARS-FS), Friedreich's Ataxia Rating Scale Activities of Daily Living (FARS-ADL), and estimated duration (Est-Dur) are shown for SCA1 (A–D) and SCA3 (E–H). Correlation coefficients (*r*) were computed using all participants' data (ataxic SCA, preataxic SCA, controls). All correlations had $p < 0.001$. FA = fractional anisotropy; ICP = inferior cerebellar peduncle; L = left; MD = mean diffusivity; mI = *myo*-inositol; R = right; SCP = superior cerebellar peduncle; tCr = total creatine; tNAA = total *N*-acetylaspartate.

microstructural (for SCA3) MR metrics detect preataxic abnormalities with exceptionally high sensitivity (AUC > 0.9 in ROC analyses) in a multisite trial setting, that they are more sensitive than structural metrics to the earliest changes, and that neurochemical and microstructural metrics are the strongest correlates of ataxia symptoms, activities of daily living, and estimated ataxia duration. Most importantly, the data demonstrate the possibility of enriching clinical trial cohorts with those individuals with the highest cerebral and cerebellar impairment before ataxia onset (detectable on a single subject level), which is currently not possible based on any clinical or laboratory measurements.

First-in-human testing of gene-silencing therapies has begun for SCA3.[44] Interventions are most likely to slow pathological changes if administered before substantial neurodegeneration,[5] and hereditary SCAs will allow enrollment of mutation carriers in clinical trials before ataxia onset. Functional changes have been documented at the preataxic stage in SCAs using dopamine transporter[45] and metabolic[46] imaging. Due to broader availability of MR scanners, we aimed to identify MR endpoints sensitive to early pathology in the trial setting for SCAs, that is, academic hospitals that house specialized ataxia clinics, which allowed us to implement a state-of-the-art MR protocol at 3T with advanced pulse sequences. The novel combination of morphometric with microstructural and neurochemical markers allowed a broader window into early pathology than prior multisite MR studies of morphometric changes in SCAs.[8,47,48] We chose ROI-based volumetric and diffusion MRI analyses to identify robust subject-level metrics for use in clinical trials. Future group-level analyses of the same data, for example, using tractography, will likely identify additional affected areas. The MRS data were limited to 2 VOIs because SCA–control classifications are driven strongly by metabolite levels in these regions.[12]

We took a conservative statistical approach, because the goal was to identify the most robust metrics that may facilitate enrollment of mutation carriers in trials, rather than to provide a detailed account of MR-detectable abnormalities. For example, we did not average right and

left volumes or combine multiple cerebellar lobules to reduce the number of statistical comparisons. To allow readers access to the full set of findings, we provide adjusted and unadjusted p values (Supplementary Materials). In addition, we primarily utilized univariate statistical analysis, because the sample size was still limited for a training and testing set needed to validate a multivariate statistical model, for example, to establish an MR score for SCA1 and SCA3.

Atrophy in the brainstem, cerebellum, and SCPs in the ataxic groups was consistent with prior reports (see Fig 1).[8,13,49,50] Notably, the WM of the cerebellum was atrophied, whereas total cerebellar cortex was not, indicative of axonopathy that precedes cell loss. Together with the microstructural damage in all cerebellar peduncles and brainstem (PCT), these data support WM deficits as the defining features of early stage pathology in both diseases. Interestingly, RD differences were more prominent than AD differences in both SCAs, indicating more prevalent myelin loss than axonal injury.[51,52] Although this interpretation is problematic in regions with many crossing fibers,[52,53] in highly ordered WM tracts, such as those in SCP (FA $\sim$ 0.67), and in the absence of edema, the prominent RD abnormalities are supportive of early oligodendrocyte pathology proposed in SCA3.[54,55]

Early GM damage was limited to select regions of the cerebellar cortex, namely lobules involved in motor processing (IV, I/II) and vestibulocerebellum (lobule X)[56] and subcortical forebrain structures (thalamus, pallidum, putamen, nucleus accumbens). Importantly, despite large overlap in cerebellar/brainstem regions involved in SCA1 and SCA3, the pattern of tissue damage was genotype-specific; therefore, imaging data collected in clinical trials should not be pooled across genotypes.

Cerebral involvement was detected with higher sensitivity by diffusion than structural MRI, consistent with microstructural changes preceding tissue loss. Prior work had shown damage to cerebral WM tracts, for example, CC and CST, in more advanced cohorts with SCA1 and SCA3.[7,57] The current study revealed the presence of these WM alterations earlier in the disease course.

At the preataxic stage, brainstem atrophy was consistent with prior reports.[7–9,49] SCP volume was the top volumetric metric that distinguished preataxic participants from controls (see Fig 4). Microstructural damage was limited to brainstem (PCT) and cerebellar tracts (ICP) in SCA1, but widespread in SCA3, before ataxia onset. Although cerebellar peduncle and midbrain WM damage was reported before ataxia onset in SCA3,[7] extended cerebral microstructural abnormalities captured in our larger preataxic cohort show that whole brain WM damage is substantial before ataxia onset in SCA3. In addition to larger sample size, the preataxic SCA3 group may have been closer to ataxia onset than the preataxic SCA1 group (see Table), allowing the detection of more extensive WM damage. However, a systematic bias in the estimated time to ataxia onset is likely for the SCA3 cohort based on the inconsistency between the estimated and reported time from onset (9 vs 3 years) in the ataxic SCA3 group. Ongoing follow-up of the preataxic patients will reveal whether the preataxic SCA3 group was closer to onset. Interestingly, diffusion measures in the ICP were the top DTI metrics that distinguished preataxic from control groups, with AUC > 0.9, for both SCAs, demonstrating impaired spinal input to the cerebellum as a very early event in the disease course. A caudal–rostral progression of SCA3 pathology was proposed previously,[7] and our findings are supportive of this sequence of events for both SCA1 and SCA3, with pathology moving from the medulla to pons, cerebellum, and later cerebrum. In this sequence of events, pontine tissue loss and neurochemical abnormalities were more extensive in preataxic SCA1 than SCA3, possibly predictive of faster disease progression in SCA1 following ataxia onset. Notably, the pontine tCr level distinguished the preataxic SCA1 subjects from controls with the highest AUC among all MR metrics, consistent with our preliminary observation that *individual* mutation carriers can be distinguished from controls based on MRS.[12] This opens the possibility of enriching clinical trial cohorts with those individuals with the highest impairment before ataxia onset. Although clinical disease manifestations can be detected before ataxia onset with larger sample sizes,[9] and preataxic sensory and corticospinal signs were detected in the larger clinical READISCA cohort (N = 200) (Tezenas du Montcel et al, Neurology, in press), COAs were not significantly different in the preataxic groups than controls with the current sample size, demonstrating the higher sensitivity of the imaging markers to early disease.

It is important for imaging markers to be related to the clinical presentation for their utility as clinically meaningful outcome measures in trials. We detected strong associations ($|r| > 0.7$) of brainstem and cerebellar MR metrics with ataxia despite a limited SARA range. Correlations of macro- and microstructural metrics obtained in the pons, cerebellar peduncles, and cerebellar WM and neuroglial markers tNAA and mI in the pons and cerebellar WM particularly stood out, underlining the importance of cerebellar afferent and efferent pathways in early symptomatology in both SCAs. MR–COA correlations were weaker overall for SCA3 than SCA1, potentially due to phenotypic heterogeneity characteristic of SCA3, which may be associated with varying MRI signatures.[58] Also note that the markers most sensitive to preataxic

pathology (eg, tCr) may not be the most sensitive to progression (eg, tNAA, the strongest neurochemical correlate of SARA), consistent with our experience in SCA1 mouse models.[59,60]

Patient-reported outcome measures are particularly important for US Food and Drug Administration approval of new therapeutics. FARS-ADL evaluates the impact of ataxia symptoms on daily activities such as speech, swallowing, and motor function (dressing, hygiene, mobility) as reported by patients and their families, and as such showed a very similar pattern of associations with MR metrics to SARA and FARS-FS. On the other hand, EQ-5D, which combines multiple domains including mobility, pain, and mental health, and the depression/anxiety scale PHQ-9 were not associated with MR metrics in SCA1 and weakly associated with few structural and neurochemical measures in SCA3. The CCAS,[21] which was designed to detect and quantify the set of impairments identified in patients with cerebellar disorders, showed a higher number of correlations with MR metrics, primarily in the cerebellum and pons.

We further observed moderate-to-strong associations of cerebellar and pons MR metrics with estimated ataxia duration. Existing statistical models to estimate time to ataxia onset in preataxic individuals utilize CAG repeat length and current age.[17,18] Although they perform well at the group level, these estimates carry a large uncertainty in estimating onset age of individual patients. Noninvasive imaging metrics can enrich these parametric models and are expected to reduce the uncertainty of these estimates, which will be critical in subject stratification in trials. The predictive value of MR metrics for ataxia onset will be better understood with longitudinal follow-up data that are currently being collected in the READISCA project.

A limitation of the study was the smaller sample size in the SCA1 group, but the ratio of SCA1 and SCA3 sample sizes was consistent with prior multisite studies.[1] The smaller sample size in SCA1 coupled with a conservative type I error correction could have limited several MR metrics to reach statistical significance. Future studies need to collect trial readiness data with larger sample sizes in global efforts such as the Ataxia Global Initiative.[61] A technical limitation was the use of scanners from a single vendor. Future trial readiness studies need to incorporate scanners from all major MR vendors. The use of state-of-the-art technologies will likely be limited in multisite settings that prioritize inclusion of all vendors and scanner models with wide-ranging technical specifications. However, the high resolution utilized here for structural imaging, the basic DTI model for analyzing only the low b value of the diffusion data, and the neurochemicals of primary interest (tNAA, mI, tCr) will be broadly appliable across vendors and models.

To summarize, morphometric, microstructural, and neurochemical metrics are highly sensitive to pathology before ataxia onset and are associated with patients' daily experiences. Neurochemical and microstructural metrics detected cerebellar and brainstem abnormalities at the preataxic stage with higher sensitivity than morphometric measures. Noninvasive access to such microstructural and biochemical changes before neuronal loss is expected to facilitate clinical trial enrollment of participants at the earliest disease stages, thereby increasing the likelihood of slowing pathological changes by potential therapeutics.

Acknowledgments

This work was supported by the NIH National Institute of Neurological Disorders and Stroke (grant U01 NS104326). The Center for Magnetic Resonance Research is supported by the National Institute of Biomedical Imaging and Bioengineering (grant P41 EB027061) and the Institutional Center Cores for Advanced Neuroimaging (awards P30 NS076408 and S10 OD017974). Research reported in this publication was also supported by an Academic Investment Research Program award at the University of Minnesota and the National Center for Advancing Translational Sciences of the NIH (award UL1TR000114). A portion of this work was performed in the McKnight Brain Institute of the University of Florida at the National High Magnetic Field Laboratory's Advanced Magnetic Resonance Imaging and Spectroscopy Facility, which is supported by the National Science Foundation (cooperative agreement DMR-1644779) and the State of Florida and was supported in part by an NIH award (S10 OD021726) for High End Instrumentation. The content is solely the responsibility of the authors and does not necessarily represent the official views of the NIH.

The READISCA investigators thank all participants for their enduring willingness and interest in this research. We extend gratitude to B. Hanna for developing the defacing/deidentification Docker pipeline, D. Hutter, A. Fishman, J. Macmore, B. Jacoby, S. Pierce, J. Magenheim, A. Ruehling, and H. Hurmic for study coordination, and C. Potvin for outstanding project management.

Author Contributions

S.T.d.M., T.A., C.L., and G.Ö. contributed to conception and design of the study. All authors contributed to acquisition or analysis of data. J.C., E.P., C.L., and G.Ö. contributed to drafting the manuscript and preparing the figures. In addition, members of the READISCA Consortium contributed to the collection of clinical data (Table S8).

Potential Conflicts of Interest

S.T.d.M. and C.L. receive research support from Biogen, which develops therapeutics for SCAs. J.D.S. consults for Biogen and has received support from Biohaven, which develop therapeutics for SCAs. T.A. has received grants from Biogen and participates in Biohaven clinical trials. Within the past 24 months, T.K. has received consulting fees from Biogen, UCB, and Vico Therapeutics, which are developing therapeutics for SCAs. G.Ö. consults for IXICO Technologies Limited, which provides neuroimaging services and digital biomarker analytics to biopharmaceutical firms conducting clinical trials for SCAs, and receives research support from Biogen, which develops therapeutics for SCAs.

References

1. Ashizawa T, Figueroa KP, Perlman SL, et al. Clinical characteristics of patients with spinocerebellar ataxias 1, 2, 3 and 6 in the US; a prospective observational study. Orphanet J Rare Dis 2013;8:177.
2. Jacobi H, Bauer P, Giunti P, et al. The natural history of spinocerebellar ataxia type 1, 2, 3, and 6: a 2-year follow-up study. Neurology 2011;77:1035–1041.
3. Schols L, Bauer P, Schmidt T, et al. Autosomal dominant cerebellar ataxias: clinical features, genetics, and pathogenesis. Lancet Neurol 2004;3:291–304.
4. Ashizawa T, Öz G, Paulson HL. Spinocerebellar ataxias: prospects and challenges for therapy development. Nat Rev Neurol 2018;14:590–605.
5. Rubinsztein DC, Orr HT. Diminishing return for mechanistic therapeutics with neurodegenerative disease duration?: There may be a point in the course of a neurodegenerative condition where therapeutics targeting disease-causing mechanisms are futile. Bioessays 2016;38:977–980.
6. Öz G, Harding IH, Krahe J, Reetz K. MR imaging and spectroscopy in degenerative ataxias: toward multimodal, multisite, multistage monitoring of neurodegeneration. Curr Opin Neurol 2020;33:451–461.
7. Rezende TJR, de Paiva JLR, Martinez ARM, et al. Structural signature of SCA3: From presymptomatic to late disease stages. Ann Neurol 2018;84:401–408.
8. Faber J, Schaprian T, Berkan K, et al. Regional Brain and Spinal Cord Volume Loss in Spinocerebellar Ataxia Type 3. Mov Disord 2021;36:2273–2281.
9. Jacobi H, Reetz K, du Montcel ST, et al. Biological and clinical characteristics of individuals at risk for spinocerebellar ataxia types 1, 2, 3, and 6 in the longitudinal RISCA study: analysis of baseline data. Lancet Neurol 2013;12:650–658.
10. Solodkin A, Peri E, Chen EE, et al. Loss of Intrinsic Organization of Cerebellar Networks in Spinocerebellar Ataxia Type 1: Correlates with Disease Severity and Duration. Cerebellum 2011;10:218–232.
11. Park YW, Joers JM, Guo B, et al. Assessment of Cerebral and Cerebellar White Matter Microstructure in Spinocerebellar Ataxias 1, 2, 3, and 6 Using Diffusion MRI. Front Neurol 2020;11:411.
12. Joers JM, Deelchand DK, Lyu T, et al. Neurochemical abnormalities in premanifest and early spinocerebellar ataxias. Ann Neurol 2018;83:816–829.
13. Deelchand DK, Joers JM, Ravishankar A, et al. Sensitivity of Volumetric Magnetic Resonance Imaging and Magnetic Resonance Spectroscopy to Progression of Spinocerebellar Ataxia Type 1. Mov Disord Clin Pract 2019;6:549–558.
14. Clinical Trial Readiness for SCA1 and SCA3 (READISCA), NCT03487367. Available from: https://clinicaltrials.gov/ct2/show/NCT03487367.
15. Maas RP, van Gaalen J, Klockgether T, van de Warrenburg BP. The preclinical stage of spinocerebellar ataxias. Neurology 2015;85:96–103.
16. Schmitz-Hübsch T, du Montcel ST, Baliko L, et al. Scale for the assessment and rating of ataxia: development of a new clinical scale. Neurology 2006;66:1717–1720.
17. Tezenas du Montcel S, Durr A, Rakowicz M, et al. Prediction of the age at onset in spinocerebellar ataxia type 1, 2, 3 and 6. J Med Genet 2014;51:479–486.
18. Peng L, Chen Z, Long Z, et al. New Model for Estimation of the Age at Onset in Spinocerebellar Ataxia Type 3. Neurology 2021;96:e2885–e2895.
19. du Montcel ST, Charles P, Ribai P, et al. Composite cerebellar functional severity score: validation of a quantitative score of cerebellar impairment. Brain 2008;131:1352–1361.
20. Jacobi H, Rakowicz M, Rola R, et al. Inventory of Non-Ataxia Signs (INAS): validation of a new clinical assessment instrument. Cerebellum 2013;12:418–428.
21. Hoche F, Guell X, Vangel MG, et al. The cerebellar cognitive affective/Schmahmann syndrome scale. Brain 2018;141:248–270.
22. Lynch DR, Farmer JM, Tsou A, et al. Measuring Friedreich ataxia: complementary features of examination and performance measures. Neurology 2006;66:1711–1716.
23. Kroenke K, Spitzer RL, Williams JB. The PHQ-9: validity of a brief depression severity measure. J Gen Intern Med 2001;16:606–613.
24. EuroQol G. EuroQol - a new facility for the measurement of health-related quality of life. Health Policy 1990;16:199–208.
25. Park YW, Deelchand DK, Joers JM, et al. AutoVOI: real-time automatic prescription of volume-of-interest for single voxel spectroscopy. Magn Reson Med 2018;80:1787–1798.
26. Deelchand DK, Berrington A, Noeske R, et al. Across-vendor standardization of semi-LASER for single-voxel MRS at 3T. NMR Biomed 2021;34:e4218.
27. Wilson M, Andronesi O, Barker PB, et al. Methodological consensus on clinical proton MRS of the brain: Review and recommendations. Magn Reson Med 2019;82:527–550.
28. Deelchand DK, Adanyeguh IM, Emir UE, et al. Two-site reproducibility of cerebellar and brainstem neurochemical profiles with short-echo, single-voxel MRS at 3T. Magn Reson Med 2015;73:1718–1725.
29. Deelchand DK, Henry PG, Joers JM, et al. Plug-and-play advanced magnetic resonance spectroscopy. Magn Reson Med 2022;87:2613–2620.
30. Archie KA, Marcus DS. DicomBrowser: software for viewing and modifying DICOM metadata. J Digit Imaging 2012;25:635–645.
31. Milchenko M, Marcus D. Obscuring surface anatomy in volumetric imaging data. Neuroinformatics 2013;11:65–75.
32. Backhausen LL, Herting MM, Buse J, et al. Quality Control of Structural MRI Images Applied Using FreeSurfer-A Hands-On Workflow to Rate Motion Artifacts. Front Neurosci 2016;10:558.
33. Glasser MF, Sotiropoulos SN, Wilson JA, et al. The minimal preprocessing pipelines for the Human Connectome Project. Neuroimage 2013;80:105–124.
34. Bastiani M, Andersson JLR, Cordero-Grande L, et al. Automated processing pipeline for neonatal diffusion MRI in the developing Human Connectome Project. Neuroimage 2019;185:750–763.

35. Schilling KG, Blaber J, Hansen C, et al. Distortion correction of diffusion weighted MRI without reverse phase-encoding scans or field-maps. PLoS One 2020;15:e0236418.

36. Deelchand DK, Adanyeguh IM, Emir UE, et al. Two-site reproducibility of cerebellar and brainstem neurochemical profiles with short-echo, single voxel MRS at 3 T. Magn Reson Med 2015;73:1718–1725.

37. Fischl B, Salat DH, van der Kouwe AJ, et al. Sequence-independent segmentation of magnetic resonance images. Neuroimage 2004;23: S69–S84.

38. Iglesias JE, Van Leemput K, Bhatt P, et al. Bayesian segmentation of brainstem structures in MRI. Neuroimage 2015;113:184–195.

39. Romero JE, Coupe P, Giraud R, et al. CERES: A new cerebellum lobule segmentation method. Neuroimage 2017;147:916–924.

40. Sörös P, Wölk L, Bantel C, et al. Replicability, Repeatability, and Long-term Reproducibility of Cerebellar Morphometry. Cerebellum 2021;20:439–453.

41. Cabeza-Ruiz R, Velazquez-Perez L, Linares-Barranco A, Perez-Rodriguez R. Convolutional Neural Networks for Segmenting Cerebellar Fissures from Magnetic Resonance Imaging. Sensors 2022;22: 1345.

42. Papinutto ND, Maule F, Jovicich J. Reproducibility and biases in high field brain diffusion MRI: An evaluation of acquisition and analysis variables. Magn Reson Imaging 2013;31:827–839.

43. Provencher SW. Estimation of metabolite concentrations from localized in vivo proton NMR spectra. Magn Reson Med 1993;30: 672–679.

44. Biogen. A Pharmacokinetics and Safety Study of BIIB132 in Adults With Spinocerebellar Ataxia 3, NCT05160558. 2021. Available from: https://clinicaltrials.gov/ct2/show/NCT05160558.

45. Yen TC, Tzen KY, Chen MC, et al. Dopamine transporter concentration is reduced in asymptomatic Machado-Joseph disease gene carriers. J Nucl Med 2002;43:153–159.

46. Soong BW, Liu RS. Positron emission tomography in asymptomatic gene carriers of Machado-Joseph disease. J Neurol Neurosurg Psychiatry 1998;64:499–504.

47. Schulz JB, Borkert J, Wolf S, et al. Visualization, quantification and correlation of brain atrophy with clinical symptoms in spinocerebellar ataxia types 1, 3 and 6. Neuroimage 2010;49:158–168.

48. Reetz K, Costa AS, Mirzazade S, et al. Genotype-specific patterns of atrophy progression are more sensitive than clinical decline in SCA1, SCA3 and SCA6. Brain 2013;136:905–917.

49. Nigri A, Sarro L, Mongelli A, et al. Spinocerebellar Ataxia Type 1: One-Year Longitudinal Study to Identify Clinical and MRI Measures of Disease Progression in Patients and Presymptomatic Carriers. Cerebellum 2022;21:133–144.

50. Piccinin CC, Rezende TJR, de Paiva JLR, et al. A 5-Year Longitudinal Clinical and Magnetic Resonance Imaging Study in Spinocerebellar Ataxia Type 3. Mov Disord 2020;35:1679–1684.

51. Song SK, Sun SW, Ramsbottom MJ, et al. Dysmyelination revealed through MRI as increased radial (but unchanged axial) diffusion of water. Neuroimage 2002;17:1429–1436.

52. Winklewski PJ, Sabisz A, Naumczyk P, et al. Understanding the Physiopathology Behind Axial and Radial Diffusivity Changes-What Do We Know? Front Neurol 2018;9:92.

53. Wheeler-Kingshott CA, Cercignani M. About "axial" and "radial" diffusivities. Magn Reson Med 2009;61:1255–1260.

54. Ramani B, Panwar B, Moore LR, et al. Comparison of spinocerebellar ataxia type 3 mouse models identifies early gain-of-function, cell-autonomous transcriptional changes in oligodendrocytes. Hum Mol Genet 2017;26:3362–3374.

55. Schuster KH, Zalon AJ, Zhang H, et al. Impaired Oligodendrocyte Maturation Is an Early Feature in SCA3 Disease Pathogenesis. J Neurosci 2022;42:1604–1617.

56. Baumann O, Borra RJ, Bower JM, et al. Consensus paper: the role of the cerebellum in perceptual processes. Cerebellum 2015;14: 197–220.

57. Martins Junior CR, Borba FC, Martinez ARM, et al. Twenty-five years since the identification of the first SCA gene: history, clinical features and perspectives for SCA1. Arq Neuropsiquiatr 2018;76:555–562.

58. Nunes MB, Martinez AR, Rezende TJ, et al. Dystonia in Machado-Joseph disease: Clinical profile, therapy and anatomical basis. Parkinsonism Relat Disord 2015;21:1441–1447.

59. Öz G, Nelson CD, Koski DM, et al. Noninvasive detection of presymptomatic and progressive neurodegeneration in a mouse model of spinocerebellar ataxia type 1. J Neurosci 2010;30:3831–3838.

60. Emir UE, Brent Clark H, Vollmers ML, et al. Non-invasive detection of neurochemical changes prior to overt pathology in a mouse model of spinocerebellar ataxia type 1. J Neurochem 2013;127:660–668.

61. Klockgether T, Ashizawa T, Brais B, et al. Paving the Way Toward Meaningful Trials in Ataxias: An Ataxia Global Initiative Perspective. Mov Disord 2022;37:1125–1130.